DEPARTMENT OF PHYSICS
UNIVERSITY OF JYVÄSKYLÄ
RESEARCH REPORT No. 2/2012

# SUPERNOVA-NEUTRINO INDUCED REACTIONS ON MOLYBDENUM VIA NEUTRAL-CURRENTS

**BY**
**EMANUEL YDREFORS**

Academic Dissertation
for the Degree of
Doctor of Philosophy

*To be presented, by permission of the*
*Faculty of Mathematics and Natural Sciences*
*of the University of Jyväskylä,*
*for public examination in Auditorium FYS1 of the*
*University of Jyväskylä on March 2, 2012*
*at 12 o'clock noon*

Jyväskylä, Finland
March 2012

# Preface

The work presented in this thesis was performed at the Department of Physics at the University of Jyväskylä during the years 2008 to 2011. The research has been founded by the University of Jyväskylä, the Graduate School in Particle and Nuclear Physics (GRASPANP) and the Ellen and Artturi Nyyssönen Foundation.

I would like to thank my supervisor Prof. Jouni Suhonen for introducing me to the realm of theoretical nuclear physics and for the excellent guidance of the research project. I also want to acknowledge Dr. Mika Mustonen for many fruitful discussions concerning nuclear theory and neutrino physics. I also want to thank my examiners Prof. Cristina Volpe and Prof. Jonathan Engel for reviewing the manuscript.

Lastly, I want to express my gratitude to my family and several other friends for all their support and encouragement.

Jyväskylä, January 2012

Emanuel Ydrefors

# Abstract

In this thesis which consists of an introductory part and six publications the neutral-current neutrino-nucleus scatterings off the stable molybdenum nuclei are studied using microscopic nuclear models. The main focus is on supernova neutrinos and the nuclear responses to them for the aforementioned nuclei are computed by folding the computed cross sections with realistic neutrino-energy spectra.

In this work both the coherent and incoherent contributions to the cross sections are considered. The contributions from the prominent multipole channels to the incoherent cross sections are also discussed in great detail.

**Author's address** Emanuel Ydrefors
Department of Physics
University of Jyväskylä
Finland

**Supervisor** Professor Jouni Suhonen
Department of Physics
University of Jyväskylä
Finland

**Reviewers** Professor Cristina Volpe
Institut de Physique Nucléaire
University of Orsay
France

Professor Jonathan Engel
Department of Physics and Astronomy
University of North Carolina
USA

**Opponent** Professor Karl-Heinz Langanke
GSI Helmholtzzentrum für Schwerionenforschung
Germany

# Publications

I. E. Ydrefors, M. T. Mustonen and J. Suhonen, *MQPM description of the structure and beta decays of the odd A=95, 97 Mo and Tc isotopes*, Nucl. Phys. A **842** (2010) 33-47.

II. E. Ydrefors and J. Suhonen, *Theoretical estimates of responses to supernova neutrinos for the stable molybdenum isotopes*, AIP conf. proc. **1304** (2010) 432-436.

III. E. Ydrefors, K. G. Balasi, J. Suhonen and T. S. Kosmas, *Nuclear Responses to Supernova Neutrinos for the Stable Molybdenum Isotopes*, in: J. P. Greene (Ed.), *Neutrinos: Properties, Reactions, Sources and Detection*, Physics Research and Technology, Nova Science Publishers, 2011.

IV. E. Ydrefors, K. G. Balasi, T. S. Kosmas and J. Suhonen, *The nuclear response of* $^{95,97}$*Mo to supernova neutrinos*, Nucl. Phys. A **866** (2011) 67-78. Erratum to appear in Nucl. Phys. A.

V. K. G. Balasi, E. Ydrefors and T. S. Kosmas, *Theoretical study of neutrino scattering off the stable even Mo isotopes at low and intermediate energies*, Nucl. Phys. A **868-869** (2011) 82-98.

VI. E. Ydrefors and J. Suhonen, *The nuclear response of molybdenum to supernova neutrinos*. Accepted for publication in AIP conf. proc.

The author of the present thesis has performed the numerical calculations for the listed publications and written the first draft of publications I, II, III, IV and VI and parts of the manuscript for V. The author has derived the expressions for the neutral-current transition densities in the microscopic quasiparticle-phonon model (MQPM). The author has implemented computer codes for calculation of transition densities and the cross sections for neutral-current neutrino scattering off nuclei.

# Contents

# 1 Introduction

The history of neutrino physics began already in 1930 when W. Pauli proposed the neutrino to explain the missing energy in nuclear beta decay. The neutrino and its properties have since then been a rapidly expanding research field with e.g. the observations of the non-zero neutrino mass and neutrino flavour oscillations [1], see [2] for a review. There are however still many open questions such as e.g. the unknown value of the neutrino mass, the Dirac-or-Majorana nature of the neutrino and the value of the third neutrino mixing angle.

From the astrophysical point of view neutrinos and neutrino-nucleus reactions play important roles in e.g. supernova explosions and for the nucleosynthesis of the heavy elements [3, 4]. Neutrinos interact only weakly with matter and neutrinos from astrophysical sources can therefore be detected by Earth-bound detectors by using neutral-current and charged-current neutrino-nucleus reactions. Supernova neutrinos therefore constitute valuable probes of both the unknown supernova mechanisms and neutrino properties [5]. One example of a possibility for future measurements is the MOON (Mo Observatory of Neutrinos) project [6]. In this experiment the neutrinos will be measured by using both charged-current and neutral-current neutrino-nucleus scattering. Observations of the neutral-current induced neutrino-nucleus reactions are important in order to test the effects of neutrino oscillations on the measured energy spectra of the electrons produced by inversed beta decays [7].

Nuclear responses to neutrinos are important both for measurements and as inputs in supernova simulations [8]. Neutral-current neutrino-nucleus scattering is independent of the neutrino flavour and can therefore be adopted also for detection of muon and tau neutrinos. Neutral-current detectors such as the OMNIS (Observatory for Multiflavor NeutrInos from Supernova) [9] or the LAND (Lead Astronomical Neutrino Detector) [10] could therefore be used to test current supernova models and to study neutrino oscillations. The purpose of this work is therefore to study neutral-current neutrino scattering off open-shell nuclei. The calculations presented in this thesis are based on the Donnelly-Walecka method [11, 12] for the treatment of semi-leptonic processes in nuclei. In its original form the theory was written in the isospin formalism. As part of this thesis the theory therefore has been formulated in the proton-neutron formalism which is more suitable for the treatment of heavy open-shell nuclei.

As the main application of our theory framework the cross sections for the neutrino scatterings off the stable ($A = 92, 94, 95, 96, 97, 98, 100$) molybdenum isotopes are

calculated. It should however be noted that the tools presented in this thesis could be applied to other nuclear systems as well.

In addition, the $^{100}$Mo nucleus is a famous double-beta-decay emitter and has been used by several current experiments e.g. the NEMO (Neutrino Ettore Majorana Observatory) [13]. Thus nuclear-structure calculations in the Mo region are welcome from many points of view. The obtained nuclear wave functions are essential in studies of weak processes in $^{100}$Mo and in the other stable molybdenum nuclei. In the case of the neutrino-nucleus scattering the cross sections are derived from these wave functions and then folded with the appropriate neutrino spectra in order to obtain realistic estimates for the nuclear responses to supernova neutrinos.

An accurate description of the final and initial nuclear states is a key ingredient in realistic neutrino-nucleus scattering calculations. In the following work the quasiparticle random-phase approximation (QRPA) [14] is adopted for the even-even isotopes. The possibility of using large valence spaces means that the QRPA and its extensions, e.g. the MAVA model [15], constitute therefore the most feasible models for the construction of vibrational states in heavy open-shell nuclei [16]. For the odd nuclei ($^{95}$Mo and $^{97}$Mo) the nuclear states are constructed by using the microscopic quasiparticle-phonon model (MQPM) [17].

# 2 Neutral-current neutrino scattering off nuclei

The calculations in this thesis are based on the so-called Donnelly-Walecka formalism for the treatment of semi-leptonic processes in nuclei. The general theory is outlined in the comprehensive work by J. D. Walecka [18] and the application of the formalism to neutral-current reactions in nuclei was reviewed in [12]. An extensive review of the theory in the form used in the present computations is given in [19]. In this chapter the formalism for the treatment of neutral-current neutrino-nucleus scattering therefore is only briefly summarized.

## 2.1 The semi-leptonic weak Hamiltonian

The Feynman diagram for the neutral-current neutrino scattering off a nucleus with proton number $Z$ and mass number $A$ is shown in Fig. 2.1. In this process which proceeds via the exchange of a neutral $Z^0$ boson the nuclear final state is either the same as the initial state (coherent scattering) or an excited state of the nucleus (incoherent scattering which is indicated by an asterisk). In the figure $k_\mu$ and $k'_\mu$ are the four momenta of the incoming and outgoing neutrinos and $p_\mu$ and $p'_\mu$ represent the four momenta of the initial and final nuclear states. Here the same conventions as in [19] are adopted. The four-momentum vector for the incoming neutrino therefore is written as $k_\mu = (E_k, -\mathbf{k})$ where $E_k$ is the energy and $\mathbf{k}$ is the three momentum. For the outgoing neutrino we have similarly $k'_\mu = (E_{k'}, -\mathbf{k}')$. The four momenta $p_\mu$ and $p'_\mu$ are defined correspondingly.

In the computations of this thesis the transferred four momentum $q_\mu$ fulfils $-q_\mu q^\mu \ll M_Z^2$ where $M_Z$ is the mass of the $Z^0$ boson. The complicated coupling in Fig. 2.1 can therefore to an excellent approximation be replaced by an effective four-point interaction. The nuclear matrix element of the effective weak Hamiltonian can then be cast into the form

$$\langle f|\mathcal{H}_{\rm eff}|i\rangle = \frac{G}{\sqrt{2}} \int l_\mu \mathrm{d}^3\mathbf{x} \mathrm{e}^{-\mathrm{i}\mathbf{q}\cdot\mathbf{x}} \langle f|\mathcal{J}^\mu(\mathbf{x})|i\rangle, \tag{2.1}$$

where for the neutral-current processes the coupling constant is $G = G_{\rm F} = 1.1664 \times$

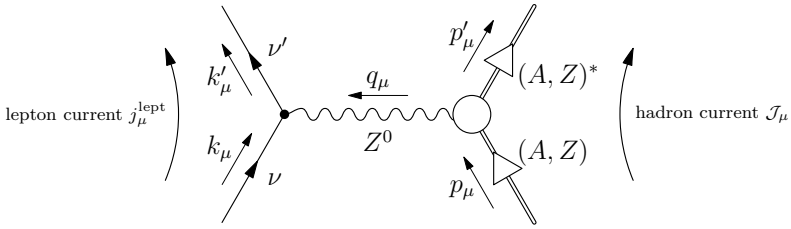


**Figure 2.1:** Neutral-current neutrino scattering off a nucleus $(A, Z)$. The transferred four momentum is here $q_\mu = k'_\mu - k_\mu$.

$10^{-5}$ GeV. In (2.1) the hadron current $\mathcal{J}^\mu(\mathbf{x})$ is of the V − A structure

$$\mathcal{J}^\mu(\mathbf{x}) = J^{\mathrm{V},\mu}(\mathbf{x}) - J^{\mathrm{A},\mu}(\mathbf{x}), \tag{2.2}$$

and $l_\mu$ is defined by

$$\langle f|j_\mu^{\rm lept}(\mathbf{x})|i\rangle = l_\mu \mathrm{e}^{-\mathrm{i}\mathbf{q}\cdot\mathbf{x}}, \tag{2.3}$$

where $j_\mu^{\rm lept}(\mathbf{x})$ represents the lepton current. At the origin ($\mathbf{x} = \mathbf{0}$) the single-nucleon matrix elements of the hadron currents $J^{\mathrm{V},\mu}(\mathbf{x})$ and $J^{\mathrm{A},\mu}(\mathbf{x})$ can be expressed in the general forms

$$\begin{aligned}{}_{\mathrm{p(n)}}\langle \mathbf{p}'\sigma'|J^{\mathrm{V},\mu}(0)|\mathbf{p}\sigma\rangle_{\mathrm{p(n)}} \\ = \frac{\bar{u}(\mathbf{p}',\sigma')}{V}\Big[F_1^{\mathrm{NC;p(n)}}(Q^2)\gamma^\mu - \frac{\mathrm{i}}{m_{\mathrm{N}}}\sigma^{\mu\nu}q_\nu F_2^{\mathrm{NC;p(n)}}(Q^2)\Big]u(\mathbf{p},\sigma),\end{aligned} \tag{2.4}$$

and

$${}_{\mathrm{p(n)}}\langle \mathbf{p}'\sigma'|J^{\mathrm{A},\mu}(0)|\mathbf{p}\sigma\rangle_{\mathrm{p(n)}} = \frac{\bar{u}(\mathbf{p}',\sigma')}{V}F_{\mathrm{A}}^{\mathrm{NC;p(n)}}(Q^2)\gamma_5\gamma^\mu u(\mathbf{p},\sigma), \tag{2.5}$$

where $|\mathbf{p}\sigma\rangle_{\mathrm{p(n)}}$ denotes the state vector of a free proton (neutron) with three-momentum $\mathbf{p}$ and spin $\sigma$ and $m_{\mathrm{N}}$ denotes the nucleon mass. In the present theory the nucleons are treated as point-like particles. The quark degree of freedom is then approximately taken into account by introducing the nucleon form factors $F_1^{\mathrm{NC;p(n)}}(Q^2)$, $F_2^{\mathrm{NC;p(n)}}(Q^2)$ and $F_{\mathrm{A}}^{\mathrm{NC;p(n)}}(Q^2)$ in (2.4) and (2.5). In this work the adopted expressions for the nucleon form factors are those of [19, 20, 21].

## 2.2 Cross-section formula for neutral-current $\nu$-nucleus scattering

The double-differential cross section for neutral-current neutrino-nucleus scattering from an initial state $i$ with angular momentum $J_i$ to a final state $f$ characterized by angular momentum $J_f$ can by a multipole expansion of 2.1 be written [18, 19]

$$\left(\frac{\mathrm{d}^2\sigma_{i\to f}}{\mathrm{d}\Omega \mathrm{d}E_{\mathrm{exc}}}\right)_{\nu/\bar{\nu}} = \frac{G_{\mathrm{F}}^2|\mathbf{k}'|E_{k'}}{\pi(2J_i+1)}\Big(\sum_{J\geqslant 0}\sigma_{\mathrm{CL}}^J + \sum_{J\geqslant 1}\sigma_{\mathrm{T}}^J\Big), \tag{2.6}$$

where

$$\begin{aligned}\sigma_{\mathrm{CL}}^J = (1+\cos\theta)\big|(J_f\|\mathcal{M}_J(q)\|J_i)\big|^2 + \big(1+\cos\theta-2b\sin^2\theta\big)\big|(J_f\|\mathcal{L}_J(q)\|J_i)\big|^2 \\ + qE_{\mathrm{exc}}(1+\cos\theta)2\mathrm{Re}\big\{(J_f\|\mathcal{M}_J\|J_i)^*(J_f\|\mathcal{L}_J(q)\|J_i)\big\},\end{aligned} \tag{2.7}$$

and

$$\begin{aligned}\sigma_{\mathrm{T}}^J = \big(1-\cos\theta+b\sin^2\theta\big)\Big(\big|(J_f\|\mathcal{T}_J^{\mathrm{mag}}(q)\|J_i)\big|^2 + \big|(J_f\|\mathcal{T}_J^{\mathrm{el}}(q)\|J_i)\big|^2\Big) \\ \mp \frac{E_k+E_{k'}}{q}(1-\cos\theta)2\mathrm{Re}\big\{(J_f\|\mathcal{T}_J^{\mathrm{mag}}(q)\|J_i)(J_f\|\mathcal{T}_J^{\mathrm{el}}(q)\|J_i)^*\big\}.\end{aligned} \tag{2.8}$$

Here $E_{\mathrm{exc}} = E_k - E_{k'}$ is the excitation energy of the nuclear final state and $\theta$ denotes the angle between the incoming and outgoing neutrinos. The magnitude of the three-momentum transfer is furthermore given by

$$q = |\mathbf{q}| = \sqrt{E_{\mathrm{exc}}^2 + 2E_kE_{k'}(1-\cos\theta)} \tag{2.9}$$

and $b = E_kE_k'/q^2$ has also been introduced. In (2.8) the minus sign is used for neutrinos and the plus sign for anti-neutrinos. The operators $\mathcal{M}_J(q)$, $\mathcal{L}_J(q)$, $\mathcal{T}_J^{\mathrm{mag}}(q)$ and $\mathcal{T}_J^{\mathrm{el}}(q)$ are the ones defined in e.g. [19].

In (2.7) and (2.8) one-body forms are assumed for the operators and they can consequently be expanded as [22]

$$T_{JM} = \widehat{J}^{-1}\sum_{ab}(a\|T_J|b)[c_a^\dagger\tilde{c}_b]_{JM}, \tag{2.10}$$

and therefore

$$(J_f\|T_J\|J_i) = \widehat{J}^{-1}\sum_{ab}(a\|T_J\|b)(J_f\|[c_a^\dagger\tilde{c}_b]_J\|J_i), \tag{2.11}$$

where the index $a$ holds the single-particle quantum numbers $n_a$, $l_a$ and $j_a$. Here $c_a^\dagger$ is the particle creation operator and the time-reversed annihilation operator $\tilde{c}_a$ is defined through the magnetic quantum number $m_\alpha$ as $\tilde{c}_\alpha = (-1)^{j_a+m_\alpha}c_{-\alpha}$ where

$-\alpha = (a, -m_\alpha)$. In (2.11) both $a$ and $b$ are either proton or neutron indices and the summations run over all single-particle orbitals in the chosen valence space. Expressions for the reduced transition densities $(J_f \| [c_a^\dagger \tilde{c}_b] \| J_i)$ for the MQPM are given in appendix A and the transition densities in the QRPA are discussed in great detail in [22].

# 3 Quasiparticle description of open-shell nuclei

In the included publications of this thesis the quasiparticle random-phase approximation (QRPA) is adopted to construct the initial and final nuclear states of the even-even isotopes. For the odd-mass nuclei ($^{95}$Mo and $^{97}$Mo) the microscopic quasiparticle-phonon model (MQPM) is used. In this chapter the quasiparticle mean-field is first introduced. The formalisms of the QRPA and the MQPM are then briefly summarized. More comprehensive treatments are given in [22] (QRPA) and in [17] (MQPM).

## 3.1 Nuclear mean field

In this thesis nuclear systems consisting of up to 100 nucleons are considered. The standard way to solve this rather involved many-body problem is to use the so-called mean-field approximation. The dominant part of the nuclear interaction is then taken into account by constructing a nuclear mean-field of non-interacting particles. The nuclear Hamiltonian with a two-body interaction $V$ is hence written as

$$H = \sum_{\alpha} \varepsilon_{\alpha} c_{\alpha}^{\dagger} c_{\alpha} + \tfrac{1}{4} \sum_{\alpha\beta\gamma\delta} \bar{v}_{\alpha\beta\gamma\delta} c_{\alpha}^{\dagger} c_{\beta}^{\dagger} c_{\delta} c_{\gamma}, \tag{3.1}$$

where $\bar{v}_{\alpha\beta\gamma\delta} = \langle \alpha\beta | V | \gamma\delta \rangle - \langle \alpha\beta | V | \delta\gamma \rangle$. Here the notation introduced in Sec. 2.2 is adopted and thus e.g. $\alpha = (a, m_{\alpha})$ with $a = (n_a, l_a, j_a)$. The single-particle energies $\varepsilon_a$ in (3.1) can either be generated by the self-consistent Hartree-Fock (HF) procedure (see e.g. [22]) or by the use of a phenomenological nuclear potential. In this work the Coulomb-corrected Woods-Saxon potential has been adopted.

An appropriate description of the pairing correlations is essential for the description of the nuclear states in open-shell nuclei. Evidence for nuclear pairing comes from e.g the odd-even mass difference and the fact that most open-shell nuclei have low-lying states of spherical shape. The foundations for the treatment of pairing phenomena in fermionic systems were laid by Bardeen, Cooper and Schrieffer [23]. The importance of pairing correlations in nuclei were first recognized by A. Bohr, B. R. Mottelson and D. Pines [24]. The BCS theory constitutes today one of the standard tools in theoretical nuclear physics. The starting point in this formalism is the ansatz for the

BCS ground state

$$|\mathrm{BCS}\rangle = \prod_{\alpha>0}\left(u_a - v_a c_\alpha^\dagger \tilde{c}_\alpha^\dagger\right)|\mathrm{HF}\rangle, \tag{3.2}$$

where the amplitudes $u_a$ and $v_a$ are solved iteratively from the BCS equations. The quasiparticles are subsequently defined via the Bogoliubov-Valatin transformation

$$\begin{cases} a_\alpha^\dagger = u_a c_\alpha^\dagger + v_a \tilde{c}_\alpha, \\ \tilde{a}_\alpha = u_a \tilde{c}_\alpha - v_a c_\alpha^\dagger. \end{cases} \tag{3.3}$$

With (3.3) the nuclear Hamiltonian (3.1) in quasiparticle representation takes the form

$$H = H_{11} + H_{02} + H_{20} + H_{13} + H_{31} + H_{40} + H_{04}, \tag{3.4}$$

where $H_{ij}$ is proportional to a normal-ordered product of $i$ quasiparticle creation operators and $j$ quasiparticle annihilation operators. In (3.4) a constant term has been omitted which anyway has no contribution to the excitation energies of interest for the present work. By the BCS procedure, i.e. by the minimization of the energy of the BCS ground state (3.2), the terms $H_{02}$ and $H_{20}$ vanish. In (3.4) the diagonal term $H_{11}$ contains most of the nucleon-nucleon short-range interactions and by the BCS approximation therefore a so-called quasiparticle mean field is introduced, i.e. a generalization of the Hartree-Fock mean-field of particles and holes. In practice the parameters of the BCS calculation however have to be fitted to reproduce the experimental pairing gaps. In this work the emperical pairing gaps have been computed from the three-point formulae [22]

$$\begin{cases} \Delta_\mathrm{p} = \frac{1}{4}(-1)^{Z+1}(S_\mathrm{p}(A+1,Z+1) - 2S_\mathrm{p}(A,Z) + S_\mathrm{p}(A-1,Z-1)), \\ \Delta_\mathrm{n} = \frac{1}{4}(-1)^{N+1}(S_\mathrm{n}(A+1,Z) - 2S_\mathrm{n}(A,Z) + S_\mathrm{n}(A-1,Z)), \end{cases} \tag{3.5}$$

by using the proton ($S_\mathrm{p}$) and neutron ($S_\mathrm{n}$) separation energies of [25]. In (3.5) $Z$ denotes the proton number and $N$ the neutron number of the even-even reference nucleus.

## 3.2 Quasiparticle random-phase approximation

In the QRPA the excited states of the even-even nucleus are constructed by coupling two-quasiparticle operators to good angular momentum $J_\omega$ and parity $\pi_\omega$. The state vector for the excitation $\omega = (J_\omega, \pi_\omega, k_\omega)$ is then given by

$$|\omega\rangle = Q_\omega^\dagger|\mathrm{QRPA}\rangle, \tag{3.6}$$

where

$$Q_\omega^\dagger = \sum_{a\leqslant a'} \sigma_{aa'}^{-1}\left(X_{aa'}^\omega \left[a_a^\dagger a_{a'}^\dagger\right]_{J_\omega M_\omega} + Y_{aa'}^\omega [\tilde{a}_a \tilde{a}_{a'}]_{J_\omega M_\omega}\right), \tag{3.7}$$

and $|\mathrm{QRPA}\rangle$ denotes the QRPA vacuum. Here $\sigma_{aa'} = \sqrt{1+\delta_{aa'}}$ and $k_\omega$ enumerates phonons with the same angular momentum and parity. In (3.7) the sum runs over all proton-proton and neutron-neutron configurations so that none of them are counted twice. The QRPA equations can be expressed in the matrix form [22]

$$\begin{pmatrix} \mathbf{A} & \mathbf{B} \\ -\mathbf{B}^* & -\mathbf{A}^* \end{pmatrix} \begin{pmatrix} \mathbf{X}^\omega \\ \mathbf{Y}^\omega \end{pmatrix} = E_\omega \begin{pmatrix} \mathbf{X}^\omega \\ \mathbf{Y}^\omega \end{pmatrix}, \tag{3.8}$$

where $\mathbf{A}$ is the well-known quasiparticle Tamm-Dancoff (QTDA) matrix and $\mathbf{B}$ contains the induced ground-state correlations. In (3.8) $E_\omega$ denotes the energy of the QRPA phonon, i.e. the excitation energy of the state $|\omega\rangle$ in a nucleus. The eigenenergies ($E_\omega$) and the eigenvectors ($\mathbf{X}^\omega$ and $\mathbf{Y}^\omega$) are then solved from (3.8) by using e.g the diagonalization method introduced by Ullah and Rowe [26].

## 3.3 Microscopic quasiparticle-phonon model

In the MQPM the building blocks are quasiparticles and QRPA phonons determined in the even-even reference nucleus adjacent to the odd-A nucleus under discussion. The states of the odd-A nucleus are then constructed by using the creation operator

$$\Gamma_k^\dagger(jm) = \sum_n X_n^k a_{njm}^\dagger + \sum_{a\omega} X_{a\omega}^k \left[a_a^\dagger Q_\omega^\dagger\right]_{jm}, \tag{3.9}$$

where $j$ denotes the angular momentum and $m$ the $z$-projection of the state. The quantum number $k$ enumerates here states with the same angular momentum and parity. The MQPM equations of motion [17] then lead to a generalized symmetric eigenvalue problem of the form

$$\mathbf{H}\boldsymbol{\psi}_{jm}^k = E_j^k \mathbf{N}\boldsymbol{\psi}_{jm}^k, \tag{3.10}$$

where $\mathbf{H}$ and $\mathbf{N}$ are the Hamiltonian matrix and the overlap matrix respectively and the components of the eigenvector $\boldsymbol{\psi}_{jm}^k$ are the amplitudes $X_n^k$ and $X_{a\omega}^k$ of (3.9). For the explicit forms of the matrices $H$ and $N$ the reader is referred to [17]. In (3.10) $E_j^k$ denotes the energy of the MQPM state. In this work the overcompleteness and non-orthogonality of the quasiparticle-phonon basis have been handled by using the diagonalization method established by Rowe [27].

# 4 Results and Discussion

In this chapter the performed calculations of the neutral-current neutrino-nucleus cross sections for the stable molybdenum isotopes upon which this thesis is based are reviewed. The computed energy spectra and wave functions are first considered in Sec. 4.1. The results for the neutrino-nucleus cross sections are subsequently discussed in Sec. 4.2.

## 4.1 Nuclear structure of the stable molybdenum isotopes

In the nuclear-structure calculations carried out for the even-even Mo isotopes in [28] and for the odd nuclei ($^{95}$Mo and $^{97}$Mo) in [29] we adopted a single-particle valence space composed of the full $3\hbar\omega$ and $4\hbar\omega$ harmonic-oscillator shells plus the $0h_{11/2}$ and $0h_{9/2}$ orbitals both for protons and neutrons. The single-particle energies were first computed from the Coulomb-corrected Woods-Saxon potential by using the parametrization by Bohr and Mottelson [30]. In the next step the quasiparticles were defined by performing BCS calculations for protons and neutrons separately. In these computations the monopole part of the interaction was scaled by a constant $g_{\rm p}^{\rm pair}$ ($g_{\rm n}^{\rm pair}$) for protons (neutrons) so that the energy of the lowest quasiparticle state was roughly equal to the emperical pairing gap $\Delta_{\rm p}$ ($\Delta_{\rm n}$) computed from (3.5). In the present calculations the Bonn one-boson-exchange potential [31] was used as the two-body interaction. The agreement between the computed BCS spectra and the available experimental level data could be improved by slightly adjusting the single-particle energies for some of the states in the vicinity of the respective Fermi surfaces. The excited states of the even-even nuclei were subsequently constructed by using the QRPA. In the QRPA calculations the particle-particle and particle-hole parts of the QRPA matrix were scaled by the parameters $g_{\rm pp}$ and $g_{\rm ph}$ respectively. For the odd-A nuclei the calculation proceeds further by the use of the MQPM. For the MQPM calculations no further adjustments of parameters were made.

In Fig. 4.1 the calculated excitation energies of $^{94}$Mo and $^{100}$Mo are shown together with the available data [32, 33]. It is seen from the figure that the results are in satisfactory agreement with the experimental energies. The obtained results are also supported by the higher-QRPA calculations performed in [34]. Here it should be noted

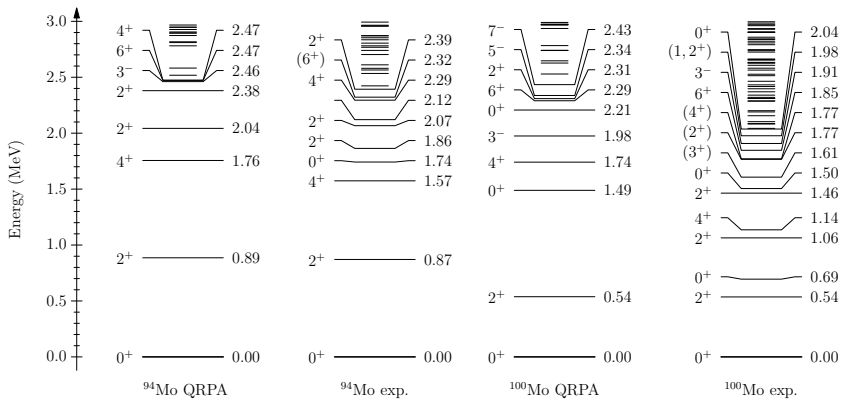


**Figure 4.1:** Comparison between the QRPA computed energy spectra and the experimental data of [32, 33] for $^{94}$Mo and $^{100}$Mo.

that it was concluded in [34] that the $2_2^+$ and $4_2^+$ states in $^{94}$Mo and the $0_2^+$ state in $^{100}$Mo are of two-phonon character.

In Fig. 4.2 the MQPM results for the energy spectra of the odd isotopes ($^{95}$Mo and $^{97}$Mo) are compared with the experimental energies of [35, 36]. It can be concluded that the agreement with the data is excellent except for the energy of the $3/2_1^+$ state in $^{95}$Mo. In [29] the quality of the MQPM wave functions were tested also by computing $\log ft$ values of beta-decay transitions from $^{95}$Tc to $^{95}$Mo and between $^{97}$Tc and $^{97}$Mo. The obtained results were in fair agreement with experimental data and the nuclear wave functions can thus be considered as a suitable starting point for neutrino-nucleus scattering calculations. The distribution of the computed states in $^{95}$Mo are displayed in Fig. 4.3. It is seen in the figure that the states are quite irregularly distributed with respect to the excitation energy $E_{\mathrm{exc}}$. This is explained by the cut of the quasiparticle-phonon basis. The same pattern is repeated for $^{97}$Mo and those results are therefore not shown here.

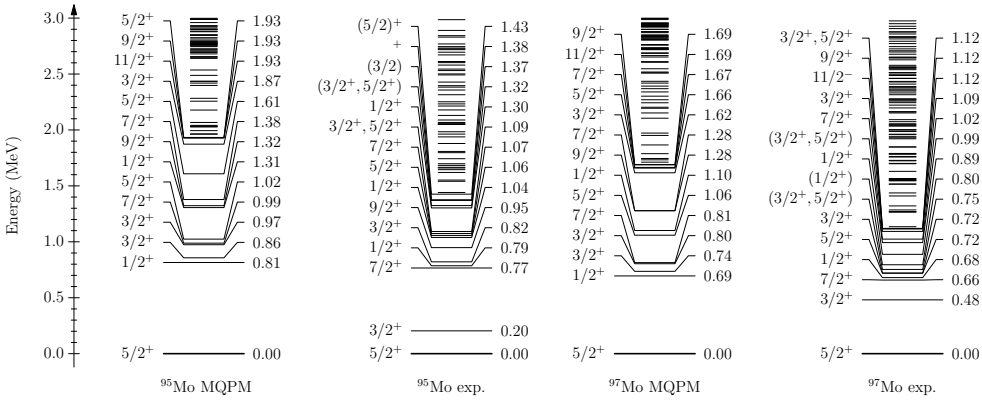


**Figure 4.2:** Comparison between the MQPM calculated energy spectra and experimental data [35, 36] for $^{95}$Mo and $^{97}$Mo.

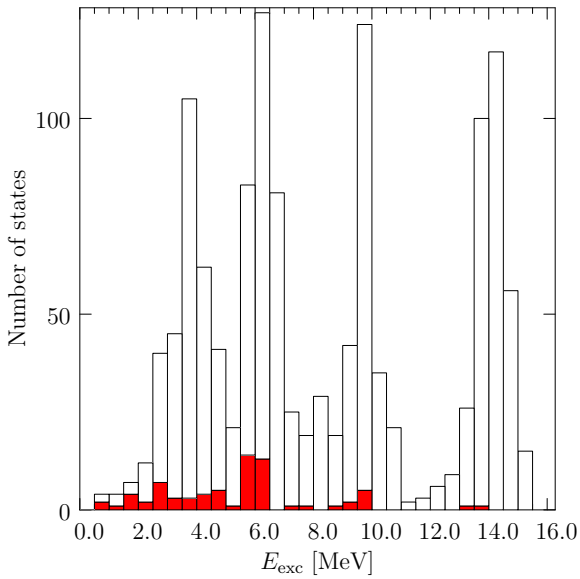


**Figure 4.3:** Distribution of the calculated states in $^{95}$Mo. In the figure the height of the bin $k$ corrreponds to the number of states having excitation energies $E_{\mathrm{exc}} \in [k\Delta E, (k+1)\Delta E]$ where $k = 0, 1, \ldots$ and $\Delta E = 0.5$ MeV. The fraction of states which contributes significantly to the neutral-current neutrino-nucleus scattering cross sections is shown in red.

## 4.2 Neutral-current neutrino-nucleus cross sections

In the papers [28, 38] we subsequently computed the cross sections for the neutral-current neutrino-nucleus scattering off the even-even and odd molybdenum isotopes respectively by using the formalism outlined in [19]. In the calculations the double-differential cross section (2.6) was first calculated for all final states $f$, scattering angles $\theta$ and neutrino energies $E_k$. The total cross section, $\sigma(E_k)$, was then computed by numerical integration over the scattering angle and subsequently adding up all the individual contributions of the included nuclear final states.

In Figs. 4.4 and 4.5 the coherent and incoherent contributions to the reactions $^{94}\mathrm{Mo}(\nu,\nu')^{94}\mathrm{Mo}^*$ and $^{95}\mathrm{Mo}(\nu,\nu')^{95}\mathrm{Mo}^*$ as functions of the energy of the incoming neutrino are shown. From the figures it can be concluded that for both reactions the total cross section is dominated by the coherent, g.s. $\longrightarrow$ g.s., transition for the neutrino energies relevant to supernova neutrinos. The same characteristics were also obtained for the other molybdenum isotopes.

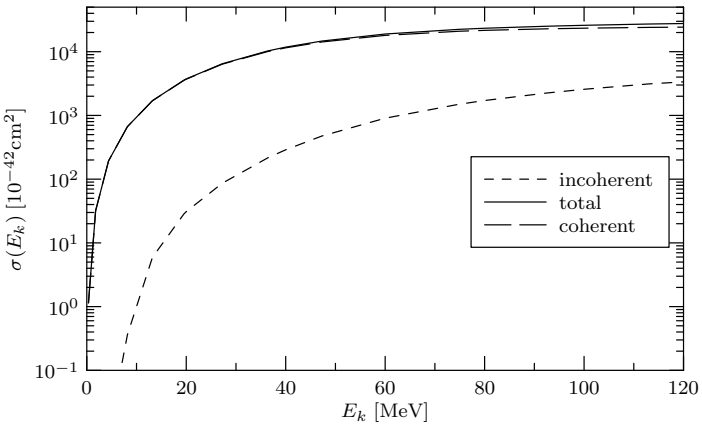


**Figure 4.4:** Coherent, incoherent and total cross sections as functions of the energy of the incoming neutrino for the neutral-current neutrino-nucleus scattering off $^{94}$Mo.

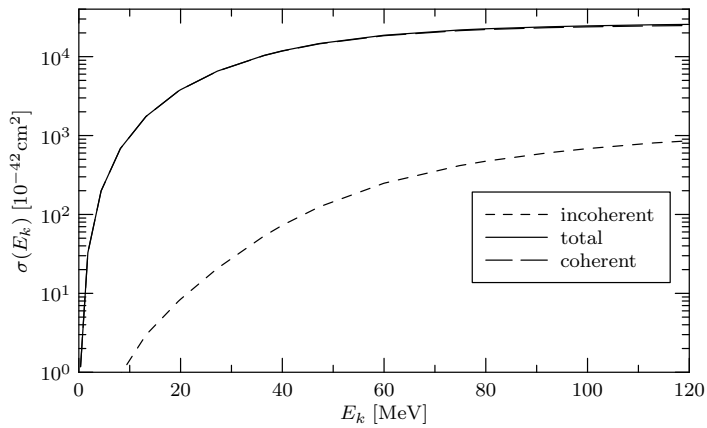


**Figure 4.5:** Coherent, incoherent and total cross sections as functions of the energy of the incoming neutrino for the reaction $^{95}$Mo$(\nu,\nu')^{95}$Mo$^*$.

In [38, 39] we studied the contributions from the possible multipole channels of (2.6) to the incoherent neutrino-nucleus cross sections. The results for $^{94}$Mo, $^{95}$Mo and $^{100}$Mo for the energies $E_k = 13.2$ MeV and $E_k = 60.0$ MeV of the incoming neutrino are presented in Figs. 4.6 and 4.7 respectively. In the figures the contributions from the axial-vector and vector components of the nuclear current (2.2) to each multipole are also shown. In Fig. 4.6 and Fig. 4.7 the contribution ("interference") coming from the mixing of the axial-vector and vector parts of the nuclear current is also displayed. It is visible in Fig. 4.6 that in the low-energy region excitations by the $1^+$ multipole are the most prominent ones for the neutral-current neutrino-nucleus scattering off $^{94}$Mo, $^{95}$Mo and $^{100}$Mo. The same conclusions holds also for the other molybdenum isotopes. The conclusion which we stated in [39] concerning the large contribution from the $0^+$ multipole to the cross sections for $^{98}$Mo and $^{100}$Mo is therefore wrong. This was caused by a minor bug found in our computer codes.

The contributions from the $1^+$ multipole for $^{98}$Mo and $^{100}$Mo are however smaller than the ones for $^{94}$Mo and $^{96}$Mo. For small neutrino energies the $1^+$ transitions proceed mainly through the operator $\mathcal{T}_1^{\mathrm{el,A}}$. The essential nuclear-structure information is thus contained in the strength functions $S_{1^+}(E_{\mathrm{exc}})$ which here have been defined as $S_{1^+}(E_{\mathrm{exc}}) = |\sqrt{6\pi}(1_f^+\|\mathcal{T}_1^{\mathrm{el,A}}(q=0.0)\|0_{\mathrm{g.s.}}^+)|^2$ for all $1^+$ final states $1_f^+$ with excitation energies $E_f$. The calculated strength functions for $^{94,96}$Mo and $^{98,100}$Mo are shown in Figs. 4.8 and 4.9 respectively. It can be concluded from the figures that for $^{94,96}$Mo most of the $1^+$ strength is coming from transitions to states with $E_{\mathrm{exc}} < 10.0$ MeV. On the other hand in $^{98}$Mo and $^{100}$Mo the bulk of the total strengths corresponds to states with $E_{\mathrm{exc}} > 10.0$ MeV. The smaller $1^+$ contributions for $^{98,100}$Mo compared to the ones of $^{94,96}$Mo are consequently explained by the fact that for the prominent $1^+$ excitations in the heaver isotopes ($^{98}$Mo and $^{100}$Mo) the energy of the outgoing

neutrino $E_{k'}$ is smaller leading to a suppression of cross sections because of the phase space factor $|\mathbf{k}'|E_{k'}$ in (2.6). From Fig. 4.7 it can furthermore be concluded that for larger neutrino energies the picture is more complicated with many contributing multipoles. In this region of neutrino energies transitions of axial-vector nature dominate the cross sections.

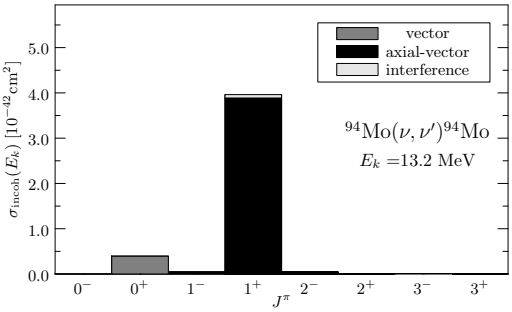


**(a)** $^{94}$Mo

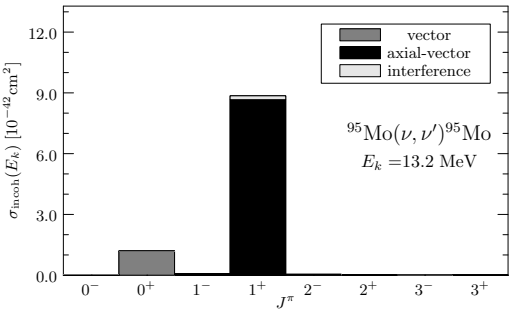


**(b)** $^{95}$Mo

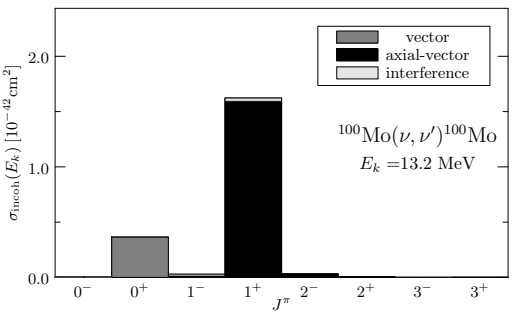


**(c)** $^{100}$Mo

**Figure 4.6:** Contributions of the dominant multipole channels to the incoherent neutrino-nucleus scattering off $^{94}$Mo, $^{95}$Mo and $^{100}$Mo for the energy $E_k = 13.2$ MeV of the incoming neutrino.

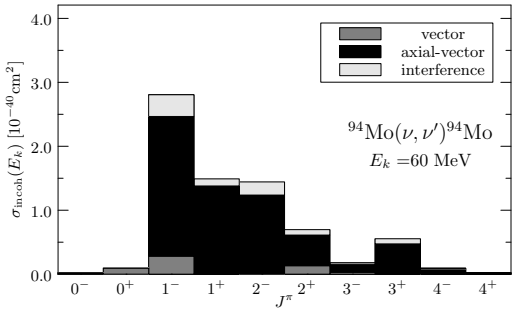


**(a)** $^{94}$Mo

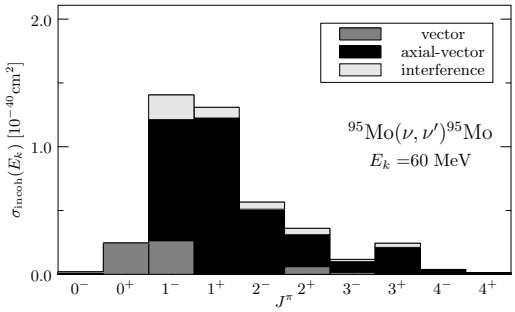


**(b)** $^{95}$Mo

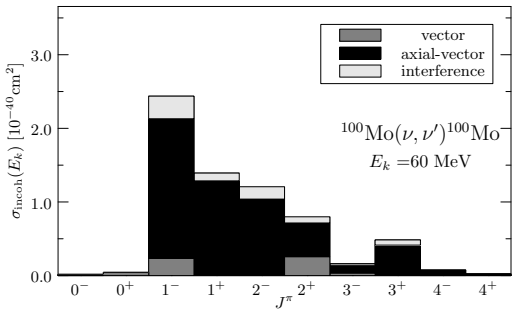


**(c)** $^{100}$Mo

**Figure 4.7:** Contributions of the dominant multipole channels to the incoherent neutrino-nucleus scattering off $^{94}$Mo, $^{95}$Mo, and $^{100}$Mo for the energy $E_k = 60.0$ MeV of the incoming neutrino.

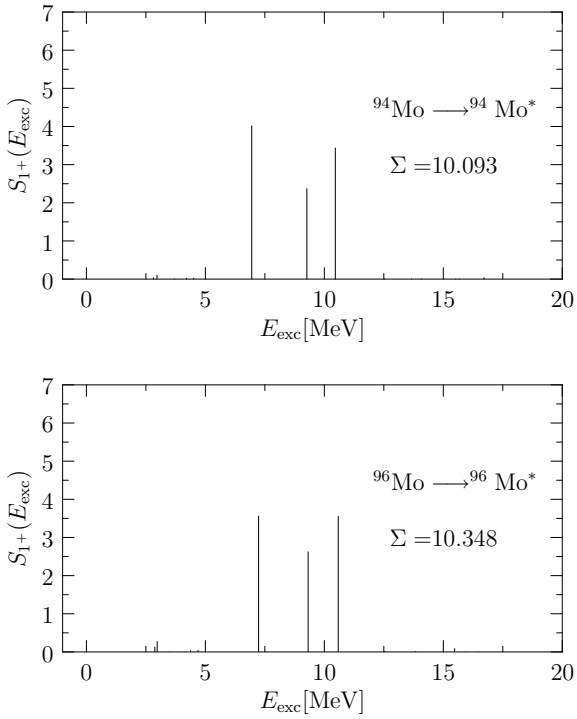


**Figure 4.8:** Computed strength functions for transitions from the QRPA ground state to excited $1^+$ states in $^{94}$Mo and $^{96}$Mo respectively.

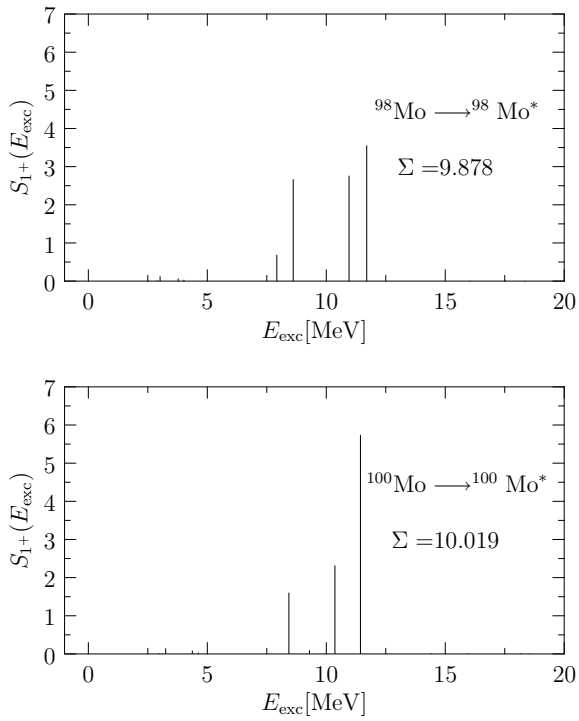


**Figure 4.9:** Computed strength functions for transitions from the QRPA ground state to excited $1^+$ states in $^{98}$Mo and $^{100}$Mo respectively.

The most important quantity from the experimental point of view is the averaged cross section, $\langle\sigma\rangle$, which is obtained by folding the total cross section $\sigma(E_k)$ with a given profile of neutrino energies. In this thesis the main focus is on the supernova neutrinos and the spectrum of neutrino energies can then be approximated by a two-parameter Fermi-Dirac distribution, i.e.

$$\langle\sigma\rangle = \frac{1}{F_2(\alpha)T^3}\int \frac{\mathrm{d}E_k\sigma(E_k)E_k^2}{\exp(E_k/T-\alpha)+1}, \tag{4.1}$$

where $T$ denotes the neutrino temperature and $\alpha$ is the degeneracy parameter. In (4.1) the neutrino flux is normalized to unity by the constant $F_2(\alpha)$. The values of $T$ and $\alpha$ employed in this work are presented in Table 4.1. In the table the corresponding average neutrino energies $\langle E_k\rangle$ are also given.

| flavour | $\alpha$ | $T$ [MeV] | $\langle E_k\rangle$ [MeV] |
|---|---|---|---|
| $\nu_e$ | 2.1 | 3.6 | 13.0 |
| $\bar{\nu}_e$ | 3.2 | 3.8 | 15.4 |
| $\nu_\mu$, $\nu_\tau$, $\bar{\nu}_\mu$, $\bar{\nu}_\tau$ | 0.8 | 4.8 | 15.7 |

**Table 4.1:** Adopted values from [40] of the parameter $\alpha$ and the neutrino temperature $T$, and the corresponding average neutrino energy $\langle E_k\rangle$ for the different neutrino flavours.

The calculated averaged cross sections for the coherent neutral-current neutrino-nucleus scattering off the stable molybdenum isotopes are shown in Table 4.2. The results for the incoherent neutrino-nucleus scattering are similarly presented in Table 4.3. From Table 4.1, Table 4.2 and Table 4.3 it is seen that both the incoherent and coherent cross sections increase significantly with increasing mean neutrino energy $\langle E_k\rangle$. As is seen in Table 4.2 the coherent cross sections for the odd nuclei ($^{95}$Mo and $^{97}$Mo) are almost the same as the ones for their even-even partners ($^{94}$Mo and $^{96}$Mo respectively). On the contrary the incoherent cross sections for $^{95}$Mo and $^{97}$Mo are slightly larger than for the even-even isotopes. The reason for this discrepancy is currently unknown.

It can also be concluded from Table 4.3 that the incoherent cross sections for $^{98}$Mo and $^{100}$Mo are smaller than the ones of the other even-even isotopes. To explain this behaviour the $0^+$ and $1^+$ contributions to the averaged cross sections for the $\nu_e$-scattering off the even-even nuclei are displayed in Fig. 4.10. As is visible in the figure the $0^+$ contribution is rather small for all the even-even isotopes It is also seen in Fig. 4.10 that the $1^+$ contribution is roughly the same for $^{92}$Mo, $^{94}$Mo and $^{96}$Mo but is notably smaller for $^{98}$Mo and $^{100}$Mo. This suppression of the $1^+$ transitions in the heavier isotopes ($^{98}$Mo and $^{100}$Mo) was discussed earlier.

It should be noted that the computed cross sections in Table 4.2 and Table 4.3 are quite sensitive to the adopted values of $T$ and $\alpha$. In [38] we showed that for tau and

muon neutrinos the calculated averaged cross sections can differ by a factor of $\sim 2-3$ depending on the adopted neutrino spectra.

| flavour | $\langle\sigma\rangle_{\rm coh}^{A=92}$ | $\langle\sigma\rangle_{\rm coh}^{A=94}$ | $\langle\sigma\rangle_{\rm coh}^{A=95}$ | $\langle\sigma\rangle_{\rm coh}^{A=96}$ | $\langle\sigma\rangle_{\rm coh}^{A=97}$ | $\langle\sigma\rangle_{\rm coh}^{A=98}$ | $\langle\sigma\rangle_{\rm coh}^{A=100}$ |
|---|---|---|---|---|---|---|---|
| $\nu_{\rm e}$ | 1.81 | 1.96 | 2.00 | 2.12 | 2.11 | 2.28 | 2.45 |
| $\bar{\nu}_{\rm e}$ | 2.40 | 2.60 | 2.66 | 2.81 | 2.81 | 3.03 | 3.26 |
| $\nu_\mu$, $\nu_\tau$ | 2.56 | 2.78 | 2.84 | 3.00 | 3.00 | 3.23 | 3.47 |
| $\bar{\nu}_\mu$, $\bar{\nu}_\tau$ | 2.56 | 2.78 | 2.83 | 3.00 | 3.00 | 3.23 | 3.47 |

**Table 4.2:** Computed averaged cross sections for the coherent neutral-current neutrino-nucleus scattering off the stable molybdenum isotopes in units of $10^{-39}$ cm$^2$. The employed values of $T$ and $\alpha$ are those given in Table 4.1.

| flavour | $\langle\sigma\rangle_{\rm incoh}^{A=92}$ | $\langle\sigma\rangle_{\rm incoh}^{A=94}$ | $\langle\sigma\rangle_{\rm incoh}^{A=95}$ | $\langle\sigma\rangle_{\rm incoh}^{A=96}$ | $\langle\sigma\rangle_{\rm incoh}^{A=97}$ | $\langle\sigma\rangle_{\rm incoh}^{A=98}$ | $\langle\sigma\rangle_{\rm incoh}^{A=100}$ |
|---|---|---|---|---|---|---|---|
| $\nu_{\rm e}$ | 11.6 | 11.8 | 16.2 | 11.9 | 16.0 | 9.94 | 8.59 |
| $\bar{\nu}_{\rm e}$ | 17.3 | 17.6 | 22.1 | 17.7 | 21.8 | 15.1 | 13.1 |
| $\nu_\mu$, $\nu_\tau$ | 25.5 | 25.3 | 28.3 | 25.3 | 27.8 | 22.1 | 19.9 |
| $\bar{\nu}_\mu$, $\bar{\nu}_\tau$ | 22.7 | 22.7 | 25.5 | 22.8 | 25.1 | 20.0 | 17.7 |

**Table 4.3:** Computed averaged cross sections for the incoherent neutral-current neutrino-nucleus scattering off the stable molybdenum isotopes in units of $10^{-42}$ cm$^2$. The employed values of $T$ and $\alpha$ are those given in Table 4.1.

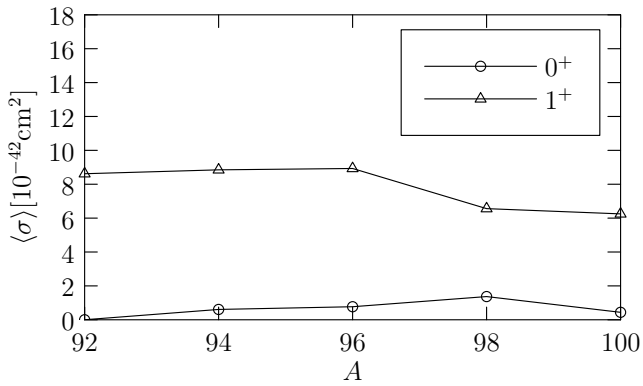


**Figure 4.10:** Contributions from the $0^+$ and $1^+$ multipoles to the nuclear responses to electron neutrinos for the even-even Mo isotopes.

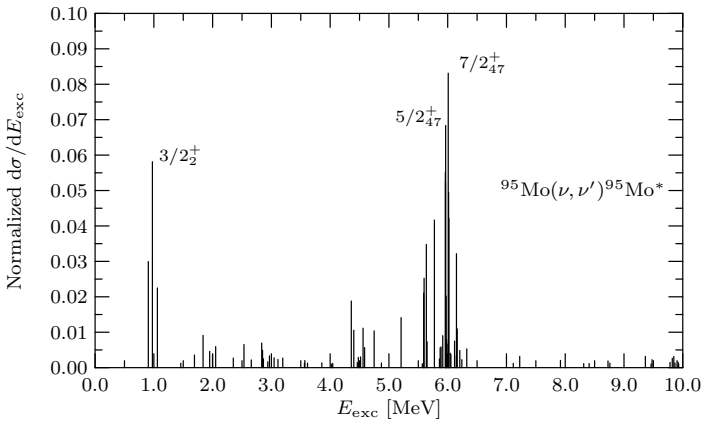


**Figure 4.11:** Differential cross sections for incoherent neutral-current neutrino-nucleus scattering to final states with excitation energy $E_{\mathrm{exc}}$ in $^{95}$Mo.

In Fig. 4.11 and Fig. 4.12 I show the differential cross sections for supernova-$\nu_{\mathrm{e}}$ scattering to various final states in $^{95}$Mo and $^{97}$Mo respectively. As we concluded in [37] the singe-particle transitions $1\mathrm{d}_{5/2} \longrightarrow 1\mathrm{d}_{3/2}$ are important. These transitions correspond to the $3/2^+_2$ and the $3/2^+_1$ states in $^{95}$Mo and $^{97}$Mo respectively. The other prominent final states in the figures are $3/2^+$, $5/2^+$ and $7/2^+$ states which are of mainly three-quasiparticle character. The most important transitions are of the form $1\mathrm{d}_{5/2} \longrightarrow 0\mathrm{g}_{9/2} \otimes \omega$ or of the form $1\mathrm{d}_{5/2} \longrightarrow 0\mathrm{g}_{7/2} \otimes \omega$ where $\omega$ stands for a QRPA phonon. In $^{97}$Mo there are also prominent transitions of either the non-spin-flip form $1\mathrm{d}_{5/2} \longrightarrow 1\mathrm{d}_{5/2} \otimes \omega$ or the spin-flip form $1\mathrm{d}_{5/2} \longrightarrow 1\mathrm{d}_{3/2} \otimes \omega$. The prominent final states can thus be interpreted as an odd neutron in the 1d orbital or as a 0g (or 1d) neutron coupled to a vibrating core. This is visualized in Fig 4.13 for $^{95}$Mo and the same reasoning holds also for $^{97}$Mo.

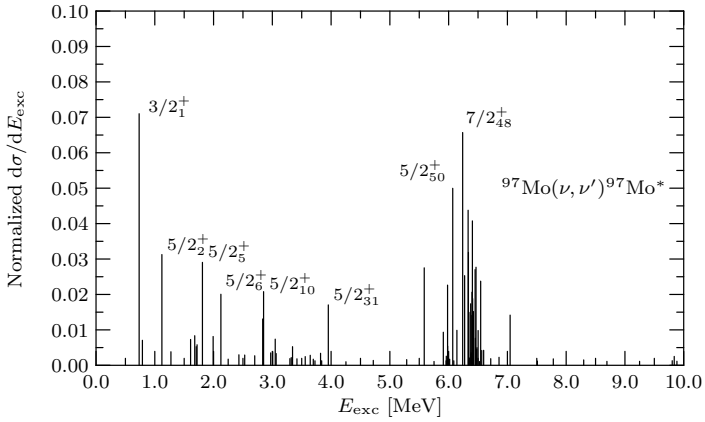


**Figure 4.12:** Differential cross sections for incoherent scattering to final states with excitation energy $E_{\text{exc}}$ in $^{97}$Mo.

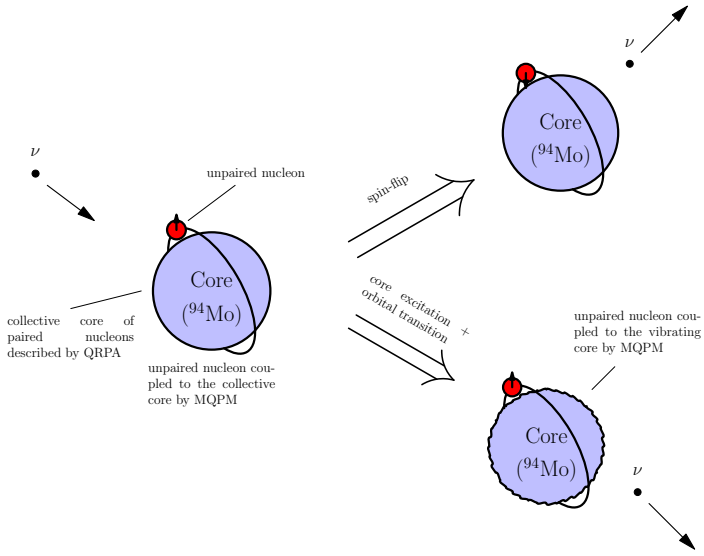


**Figure 4.13:** Neutral-current neutrino-nucleus scattering off $^{95}$Mo. In the figure the spin of the odd particle is indicated by an arrow.

# 5 Conclusions

In this thesis a comprehensive study of the neutral-current neutrino-nucleus scatterings off the stable ($A = 92, 94, 95, 96, 97, 98, 100$) molybdenum isotopes was performed. Studies of weak interaction phenomena in these nuclei are of importance for e.g. the MOON experiment planned in Japan. In this work the cross sections for the aforementioned nuclear targets were computed for neutrino energies relevant for supernova neutrinos. The nuclear responses to supernova neutrinos were subsequently calculated by folding the obtained cross sections with a two-parameter Fermi-Dirac distribution. In the computations the final and initial nuclear states of the even-even isotopes were constructed within the context of the QRPA. For the odd nuclei ($^{95}$Mo and $^{97}$Mo) the nuclear states were generated by using the microscopic quasiparticle-phonon model.

In our calculations we have found that the coherent contribution dominates the cross sections for the neutrino energies which are relevant for supernova neutrinos. For the typical energies of supernova neutrinos excitations of the $1^+$ multipole are the most important for all the studied nuclei. For neutrino energies which correspond to the high-energy tail of the neutrino spectrum similar patterns are seen for all the studied isotopes. At these energies the most important multipole is $1^-$ but also several other multipoles contribute significantly to the cross sections.

For the odd nuclei we have found that the prevalent final states can simply be thought of as an unpaired nucleon in a 1d orbital or as a 0g nucleon coupled to a vibrating core. The coherent cross sections for the odd nuclei are roughly the same as for the even-even isotopes. On the contrary the incoherent cross sections for $^{95}$Mo and $^{97}$Mo are slightly larger than for even-even nuclei. The reason for this enhancement of the cross sections for the odd isotopes is currently unknown. One aspect which needs to be studied more is how the cut of the quasiparticle-phonon basis affects the cross sections.

The computed averaged neutrino-nucleus cross sections turn out to be rather sensitive to the supernova model used. Depending on the adopted values of the neutrino parameters the nuclear responses to tau and muon neutrinos might differ by a factor of $\sim 2 - 3$. This uncertainty is probably larger than the errors coming from the nuclear-structure calculations. Future experiments can thus presumably be used to test the validity of the current supernova models.

# References


[1] Y. Fukuda et al. (Super-Kamiokande Collaboration), *Phys. Rev. Lett.* **81** (1998) 1562.

[2] C. Giunti and C. W. Kim, *Fundamentals of Neutrino Physics and Astrophysics*, Oxford University Press, New York, 2007.

[3] K. Langanke and G. Martínez-Pinedo, *Rev. Mod. Phys.* **75** (2003) 819.

[4] K. Langanke, *Acta Phys. Pol. B* **39** (2008) 265.

[5] J. Gava and C. Volpe, *AIP Conf. Proc.* **1038** (2008) 193.

[6] H. Ejiri et al., *Eur. Phys. J. Special Topics* **162** (2008) 239.

[7] H. Ejiri. Private communication.

[8] K. Langanke, *Nucl. Phys. A* **834** (2010) 608c.

[9] P. F. Smith, *Astro. Part. Phys.* **8** (1997) 27.

[10] C. K. Hargrove et al., *Astro. Part. Phys.* **5** (1996) 183.

[11] J. S. O'Connell, T. W. Donnelly and J. D. Walecka, *Phys. Rev. C* **6** (1972) 719.

[12] T. W. Donnelly and R. D. Peccei, *Phys. Rep.* **50** (1979) 1.

[13] R. Arnold et al., *Phys Rev. Lett.* **95** (2005) 182302.

[14] M. Baranger, *Phys. Rev.* **120** (1960) 957.

[15] D. S. Delion and J. Suhonen, *Phys. Rev. C* **67** (2003) 034301.

[16] P. Ring and P. Schuck, *The Nuclear Many-Body Problem*, Springer, New York, 1980.

[17] J. Toivanen and J. Suhonen, *Phys. Rev. C* **57** (1998) 1237.

[18] J. D. Walecka, *Theoretical Nuclear and Subnuclear Physics*, Imperial College Press, London, 2004.

[19] E. Ydrefors et al., "Nuclear Responses to Supernova Neutrinos for the Stable Molybdenum Isotopes", in: J. P. Greene (Ed.), *Neutrinos: Properties, Reactions, Sources and Detection*, Nova Science Publishers, 2011. Included in this thesis.

[20] W. M. Alberico, S. M. Bilenky and C. Maieron, *Phys. Rep.* **358** (2002) 227.

[21] W. M. Alberico et al., *Phys. Rev. C* **79** (2009) 065204.

[22] J. Suhonen, *From Nucleons to Nucleus: Concepts of Microscopic Nuclear Theory*, Springer, Berlin, 2007.

[23] J. Bardeen, L. N. Cooper and J. R. Schrieffer, *Phys. Rev.* **108** (1957) 1175.

[24] A. Bohr, B. R. Mottelson and D. Pines, *Phys. Rev.* **110** (1958) 936.

[25] G. Audi, A. H. Wapstra and C. Thibault, *Nucl. Phys. A* **729** (2003) 337.

[26] P. Ullah and D. J. Rowe, *Nucl. Phys. A* **163** (1971) 257.

[27] D. J. Rowe, *J. Math.* **10** (1969) 1774.

[28] K. G. Balasi, E. Ydrefors and T. Kosmas, *Nucl. Phys. A* **868-869** (2011) 82. Included in this thesis.

[29] E. Ydrefors, M. T. Mustonen and J. Suhonen, *Nucl. Phys A* **842** (2010) 33. Included in this thesis.

[30] A. Bohr and B. R. Mottelson, *Nuclear Structure, Vol. I*, Benjamin, New York, 1969.

[31] K. Holinde, *Phys. Rep.* **68** (1981) 121.

[32] D. Abriola and A. A. Sonzogni, *Nucl. Data Sheets* **107** (2006) 2423.

[33] B. Singh, *Nucl. Data Sheets* **109** (2008) 297.

[34] J. Kotila, J. Suhonen and D. S. Delion, *Nucl. Phys. A* **765** (2006) 354.

[35] T. W. Burrows, *Nucl. Data Sheets* **68** (1993) 635.

[36] A. Artna-Cohen, *Nucl. Data Sheets* **70** (1993) 85.

[37] E. Ydrefors and J. Suhonen, *AIP conf. proc.* **1304** (2010) 432. Included in this thesis.

[38] E. Ydrefors et al., *Nucl. Phys. A* **866** (2011) 67. Included in this thesis. Erratum submitted to Nucl. Phys. A.

[39] E. Ydrefors and J. Suhonen, *AIP conf. proc.* (2011). In press. Included in this thesis.

[40] M. T. Keil and G. G. Raffelt, *Astrophys. J.* **590** (2003) 971.

# A Neutral-current transition densities in the MQPM

In this appendix the reduced neutral-current transition densities in the MQPM framework are presented. In the present notation the label $p$ refers to a proton orbital and $n$ to a neutron orbital. When the indices $a$ and $b$ are adopted both of them are either proton or neutron indices. Here only the expressions for a neutron-odd nucleus are given. It is however straightforward to obtain the corresponding expressions for a proton-odd nucleus by interchanging all neutron labels into proton labels and vice versa.

In the MQPM the basis set consists of one-quasiparticle states $|\nu\rangle = |n;m\rangle = |n_n l_n j_n;m\rangle$ and quasiparticle-phonon states $|n\omega;jm\rangle$. A quasiparticle state with angular momentum $j$ and magnetic quantum number $m$ is then given by

$$|n;m\rangle = a^\dagger_\nu|\mathrm{QRPA}\rangle \tag{A.1}$$

and a quasiparticle-phonon state is defined as

$$|n\omega;jm\rangle = [a^\dagger_n Q^\dagger_\omega]_{jm}|\mathrm{QRPA}\rangle, \tag{A.2}$$

where $|\mathrm{QRPA}\rangle$ is the QRPA vacuum. The QRPA creation operator $Q^\dagger_\omega$ is here given by

$$Q^\dagger_\omega = \tfrac{1}{2}\sum_{aa'}\sigma^{-1}_{aa'}(\bar{X}^\omega_{aa'}[a^\dagger_a a^\dagger_{a'}]_{J_\omega M_\omega} + \bar{Y}^\omega_{aa'}[\tilde{a}_a\tilde{a}_{a'}]_{J_\omega M_\omega}), \tag{A.3}$$

where the auxiliary amplitudes are given by

$$\bar{X}^\omega_{aa'} = \begin{cases} X^\omega_{aa'} & \text{if } a < a', \\ 2X^\omega_{aa'} & \text{if } a = a', \\ (-1)^{j_a+j_{a'}+J_\omega+1}X^\omega_{a'a} & \text{if } a > a' \end{cases} \tag{A.4}$$

and the amplitudes $\bar{Y}^\omega_{aa'}$ are defined correspondingly. In this way the restriction $a \leqslant a'$, present in (3.7), is relaxed to simplify the calculations.

The reduced transition density for a transition between two one-quasiparticle states is given by

$$(n_f\|[c^\dagger_a\tilde{c}_b]_\lambda\|n_i) = \widehat{\lambda}(u_a u_b\delta_{an_f}\delta_{bi} + (-1)^{j_a+j_b-\lambda}v_a v_b\delta_{an_i}\delta_{bn_f}). \tag{A.5}$$

For the reduced transition densities concerning transitions between a one-quasiparticle state and a quasiparticle-phonon state the matrix elements take the forms

$$(n_f\|[c_p^\dagger\tilde{c}_{p'}]_\lambda\|n_i\omega_i;j_i) = -\delta_{n_in_f}\delta_{\lambda J_{\omega_i}}(-1)^{j_{n_f}+j_i+\lambda}\widehat{j_i}\sigma^{-1}_{pp'}\big(v_pu_{p'}\bar{X}^{\omega_i}_{pp'}+u_pv_{p'}\bar{Y}^{\omega_i}_{pp'}\big), \quad (A.6)$$

$$\begin{aligned}(n_f\|[c_n^\dagger\tilde{c}_{n'}]_\lambda\|n_i\omega_i;j_i) &= -(-1)^{j_{n_f}+j_i+\lambda}\widehat{\lambda}\widehat{j_i}\widehat{J_{\omega_i}}\Bigg[\delta_{n_fn_i}\frac{\delta_{\lambda J_{\omega_i}}}{\widehat{J_{\omega_i}}^2}\sigma^{-1}_{nn'}\big(v_nu_{n'}\bar{X}^{\omega_i}_{nn'}+u_nv_{n'}\bar{Y}^{\omega_i}_{nn'}\big)\\ &+\Bigg(\delta_{n'n_i}v_nu_{n'}\begin{Bmatrix}j_{n_f}&\lambda&j_i\\ j_{n'}&J_{\omega_i}&j_n\end{Bmatrix}\sigma^{-1}_{nn_f}\bar{X}^{\omega_i}_{nn_f}+\delta_{nn_f}\frac{\delta_{j_ij'_n}}{\widehat{j_{n'}}^2}u_nv_{n'}\\ &\times(-1)^{j_n+j_{n'}+\lambda}\sigma^{-1}_{n'n_i}\bar{Y}^{\omega_i}_{n'n_i}\Bigg)-(-1)^{j_n+j_{n'}+\lambda}\Bigg(\delta_{nn_i}v_nu_{n'}\begin{Bmatrix}j_{n_f}&\lambda&j_i\\ j_n&J_{\omega_i}&j_{n'}\end{Bmatrix}\\ &\times\sigma^{-1}_{n'n_f}\bar{X}^{\omega_i}_{n'n_f}+\delta_{n'n_f}\frac{\delta_{j_ij_n}}{\widehat{j_n}^2}v_nu_{n'}(-1)^{j_n+j_{n'}+\lambda}\sigma^{-1}_{nn_i}\bar{Y}^{\omega_i}_{nn_i}\Bigg)\Bigg], \quad (A.7)\end{aligned}$$

$$(n_f\omega_f;j_f\|[c_p^\dagger\tilde{c}_{p'}]_\lambda\|n_i) = \delta_{n_fn_i}\delta_{\lambda J_{\omega_f}}\widehat{j_f}\sigma^{-1}_{pp'}\big(u_pv_{p'}\bar{X}^{\omega_f}_{pp'}+v_pu_{p'}\bar{Y}^{\omega_f}_{pp'}\big), \quad (A.8)$$

and

$$\begin{aligned}(n_f\omega_f;j_f\|[c_n^\dagger\tilde{c}_{n'}]_\lambda\|n_i) &= \widehat{j_f}\widehat{\lambda}\widehat{J_{\omega_f}}\Bigg[\delta_{n_fn_i}\frac{\delta_{\lambda J_{\omega_f}}}{\widehat{J_{\omega_f}}^2}\sigma^{-1}_{nn'}\big(u_nv_{n'}\bar{X}^{\omega_f}_{nn'}+v_nu_{n'}\bar{Y}^{\omega_f}_{nn'}\big)+\Bigg(\delta_{n'n_f}u_nv_{n'}\\ &\times\begin{Bmatrix}j_f&\lambda&j_{n_i}\\ j_n&J_{\omega_f}&j_{n'}\end{Bmatrix}\sigma^{-1}_{nn_i}\bar{X}^{\omega_f}_{nn_i}+\delta_{nn_i}\frac{\delta_{j_fj_{n'}}}{\widehat{j_{n'}}^2}v_nu_{n'}(-1)^{j_f+j_{n_i}+\lambda}\sigma^{-1}_{n'n_f}\bar{Y}^{\omega_f}_{nn_f}\Bigg)\\ &-(-1)^{j_n+j_{n'}+\lambda}\Bigg(\delta_{nn_f}u_nv_{n'}\begin{Bmatrix}j_f&\lambda&j_{n_i}\\ j'_n&J_{\omega_f}&j_n\end{Bmatrix}\sigma^{-1}_{n'n_i}\bar{X}^{\omega_f}_{n'n_i}\\ &+\delta_{n'n_i}\frac{\delta_{j_fj_n}}{\widehat{j_n}^2}v_nu_{n'}(-1)^{j_{n_i}+j_f+\lambda}\sigma^{-1}_{nn_f}\bar{Y}^{\omega_f}_{nn_f}\Bigg)\Bigg]. \quad (A.9)\end{aligned}$$

The reduced transition density between two quasiparticle phonon states can be written on the form

$$\begin{aligned}&(n_f\omega_f;j_f\|[c_a^\dagger\tilde{c}_b]_\lambda\|n_i\omega_i;j_i)\\ &\quad= u_au_b(n_f\omega_f;j_f\|[a_a^\dagger\tilde{a}_b]_\lambda\|n_i\omega_i;j_i)+(-1)^{j_a+j_b+\lambda}v_av_b(n_f\omega_f;j_f\|[a_b^\dagger\tilde{a}_a]_\lambda\|n_i\omega_i;j_i),\end{aligned} \quad (A.10)$$

where

$$
\begin{aligned}
&(n_f\omega_f; j_f \| [a_p^\dagger \tilde{a}_{p'}]_\lambda \| n_i\omega_i; j_i) \\
&\quad = \delta_{n_f n_i} \widehat{\lambda}\widehat{J_{\omega_f}}\widehat{J_{\omega_i}}\widehat{j_f}\widehat{j_i} \begin{Bmatrix} j_f & \lambda & j_i \\ J_{\omega_i} & j_{n_f} & J_{\omega_f} \end{Bmatrix} \sum_{b'} (-1)^{j_f + j_{n_f} + j_p + j_{b'}} \sigma^{-1}_{pb'} \sigma^{-1}_{p'b'} \\
&\qquad \times \left( \begin{Bmatrix} J_{\omega_f} & \lambda & J_{\omega_i} \\ j_{p'} & j_{b'} & j_p \end{Bmatrix} \bar{X}^{\omega_f}_{pb'} \bar{X}^{\omega_i}_{p'b'} + (-1)^\lambda \begin{Bmatrix} J_{\omega_f} & \lambda & J_{\omega_i} \\ j_p & j_{b'} & j_{p'} \end{Bmatrix} \bar{Y}^{\omega_f}_{p'b'} \bar{Y}^{\omega_i}_{pb'} \right) \qquad \text{(A.11)}
\end{aligned}
$$

and

$$
\begin{aligned}
&(n_f\omega_f; j_f \| [a_n^\dagger \tilde{a}_{n'}]_\lambda \| n_i\omega_i; j_i) \\
&\quad = \widehat{J_{\omega_f}}\widehat{J_{\omega_i}}\widehat{j_f}\widehat{j_i}\widehat{\lambda} \Bigg[ \delta_{n'n_i} (-1)^{j_{n_f} + J_{\omega_f} + j_i + \lambda} \begin{Bmatrix} j_i & j_f & \lambda \\ j_n & j_{n'} & J_{\omega_i} \end{Bmatrix} \sum_{b'} \sigma^{-1}_{nb'} \sigma^{-1}_{n_f b'} \\
&\qquad \times \left( \begin{Bmatrix} j_f & J_{\omega_i} & j_n \\ j_{b'} & J_{\omega_f} & j_{n_f} \end{Bmatrix} \bar{X}^{\omega_f}_{nb'} \bar{X}^{\omega_i}_{n_f b'} - \frac{\delta_{j_{b'} j_f}}{\widehat{j_{b'}}^2} \bar{Y}^{\omega_i}_{nb'} Y^{\omega_f}_{n_f b'} \right) \\
&\qquad - \delta_{nn_f} (-1)^{J_{\omega_i} + j_{n_i} + j_n + j_{n'} + j_i + \lambda} \begin{Bmatrix} j_i & j_f & \lambda \\ j_n & j_{n'} & J_{\omega_f} \end{Bmatrix} \sum_{b'} \sigma^{-1}_{n_i b'} \sigma^{-1}_{n'b'} \\
&\qquad \times \left( \begin{Bmatrix} j_i & J_{\omega_f} & j_{n'} \\ j_{b'} & J_{\omega_i} & j_{n_i} \end{Bmatrix} \bar{X}^{\omega_f}_{n_i b'} \bar{X}^{\omega_i}_{n'b'} - \frac{\delta_{j_{b'} j_i}}{\widehat{j_{b'}}^2} \bar{Y}^{\omega_i}_{nb'} \bar{Y}^{\omega_f}_{n'b'} \right) \\
&\qquad + \delta_{n_i n_f} \begin{Bmatrix} \lambda & j_f & j_i \\ j_{n_f} & J_{\omega_i} & J_{\omega_f} \end{Bmatrix} \sum_{b'} (-1)^{j_n + j_{b'} + j_{n_f} + j_f} \sigma^{-1}_{nb'} \sigma^{-1}_{n'b'} \\
&\qquad \times \left( \begin{Bmatrix} J_{\omega_f} & J_{\omega_i} & \lambda \\ j_{n'} & j_n & j_{b'} \end{Bmatrix} \bar{X}^{\omega_f}_{nb'} \bar{X}^{\omega_i}_{n'b'} + (-1)^\lambda \begin{Bmatrix} J_{\omega_i} & J_{\omega_f} & \lambda \\ j_{n'} & j_n & j_{b'} \end{Bmatrix} \bar{Y}^{\omega_i}_{nb'} \bar{Y}^{\omega_f}_{n'b'} \right) \\
&\qquad + \sigma^{-1}_{nn_i} \sigma^{-1}_{n'n_f} \Bigg( (-1)^{J_{\omega_f} + J_{\omega_i} + j_{n'} + \lambda} \begin{Bmatrix} j_n & j_{n_i} & J_{\omega_f} \\ j_{n'} & J_{\omega_i} & j_{n_f} \\ \lambda & j_i & j_f \end{Bmatrix} \bar{X}^{\omega_f}_{nn_i} \bar{X}^{\omega_i}_{n'n_f} \\
&\qquad\qquad + (-1)^{j_n + j_f + \lambda} \frac{\delta_{j_{n'} j_f} \delta_{j_n j_i}}{\widehat{j_{n'}}^2 \widehat{j_n}^2} \bar{Y}^{\omega_i}_{nn_i} \bar{Y}^{\omega_f}_{n'n_f} \Bigg) \Bigg] \\
&\qquad\qquad + \delta_{nn_f} \delta_{n'n_i} \delta_{\omega_i \omega_f} \widehat{j_f}\widehat{j_i}\widehat{\lambda} (-1)^{j_n + j_i + J_{\omega_f} + \lambda} \begin{Bmatrix} j_i & j_f & \lambda \\ j_n & j_{n'} & J_{\omega_f} \end{Bmatrix}. \qquad \text{(A.12)}
\end{aligned}
$$

In the case then the initial ($i$) and final ($f$) states are the same also the term $\delta_{ab}\delta_{\lambda 0}\widehat{j_a} v_a^2 \widehat{j_i}$ has to be added to (A.5), (A.6), (A.7), (A.8) , (A.9) and (A.10). This is the case in e.g. coherent neutrino-nucleus scattering which is considered in this work.